

## ZnTe at high pressure: X-ray-absorption spectroscopy and x-ray-diffraction studies

A. San-Miguel, A. Polian, M. Gauthier, and J. P. Itié

*Physique des Milieux Condensés, Université Pierre et Marie Curie, B 77, 4 place Jussieu, F-75252 Paris CEDEX 05, France*

(Received 26 April 1993)

ZnTe has been studied by x-ray-absorption spectroscopy at the Zn *K* edge and by x-ray diffraction up to 30 GPa. Crystallographic transitions were observed at 9.5 and 12 GPa by both techniques. The combination of x-ray-absorption near-edge structure, extended x-ray-absorption fine structure, and diffraction analysis enables us to determine the structure of ZnTe-II which is cinnabar with two pairs of first neighbors at approximately the same distance ( $\sim 2.558$  Å at 11.7 GPa), maintaining the fourfold coordination, the third pair of neighbors being much farther ( $\sim 3.37$  Å). At 12 GPa ZnTe-II destabilizes and gives rise to a distorted rocksalt-type coordination, which remains stable at least up to 30 GPa. The succession of transitions is structurally reversible and takes place without amorphization. The hysteresis of the transitions has also been studied. A Murnaghan equation of state fitted to the values of the ZnTe cell parameter in ZnTe-I gives a bulk modulus of  $50.5 \pm 3$  GPa in good agreement with previous work.

### I. INTRODUCTION

The application of hydrostatic pressure is one of the most powerful experimental methods to test the form of the interatomic potentials as a function of distance. Among the most stringent tests for the (in)validation of models and theories are the determination of transition pressures and the computation of the molar volume variation with pressure (equation of state). The high-pressure test has been one of the great successes of pseudopotential calculations<sup>1</sup> which have been used to compute the ambient band structures of semiconductors. More recently, it has been used to test interatomic potentials that are used to study the physics of liquid phases in Ge.<sup>2</sup> An experimental effort is requested to give accurate results on transition pressures and equations of state, which can enable us to discriminate between theories in *ab initio* calculations or to give a good parametrization for semiempirical models. To make possible the computation of the transition pressures, the structure of the phases involved must be known. Moreover, as phase metastability is a common event, the study of the reverse transition is needed to delimit, in the case of hysteresis (different values for the forward and reverse transitions), the pressure domain where the thermodynamic transition takes place.

ZnTe under ambient conditions is a direct-band-gap semiconductor (2.3 eV), which crystallizes in the cubic zinc-blende structure with a lattice parameter of 6.100 Å.<sup>3</sup> The first-neighbor distance is 2.64 Å. The behavior of ZnTe under high pressure has been the focus of a variety of studies because of the existence, below 30 GPa, of a quite original phase diagram when compared with the other zinc chalcogenides (ZnS and ZnSe). Indeed, ZnS and ZnSe have a single phase transition at 15 and 13 GPa, respectively. The high-pressure phase has the sodium chloride structure with atoms in an octahedral site symmetry. In contrast, ZnTe shows two successive phase transitions near 9.5 and 12 GPa. The symmetry of the

high-pressure phases in ZnTe has led to a number of arguments, especially for ZnTe-II. The local character of these phases has never been determined. From the first high-pressure work on ZnTe by Samara and Drickamer,<sup>4</sup> three sharp changes in electrical resistivity were observed below 15 GPa. Their results indicated a metallic transition around 12 GPa in the revised pressure scale. Smith and Martin<sup>5</sup> mentioned that from their x-ray studies, only two of the resistivity changes observed by Samara and Drickamer corresponded to structural phase transitions. In a combined x-ray-diffraction and electric resistivity<sup>6,7</sup> study, structural transitions were found at approximately 8.5 GPa to a nonmetallic hexagonal phase (ZnTe-II) and 13.0 GPa to a metallic phase (ZnTe-III). A resistivity drop of four orders of magnitude which takes place near 3.0 GPa is not correlated with a structural transformation. Moreover, a broadening of the half-width of the  $\Gamma_{15}$  excitonic peak in optical absorption has been observed in ZnTe-I between 3 and 5 GPa.<sup>8</sup> This behavior has been tentatively assigned to the creation of point defects. Reflectivity measurement<sup>9</sup> confirmed the nonmetallic character of ZnTe-II and the metallic one of ZnTe-III. In an optical-absorption measurement<sup>10</sup> the values obtained for the transition pressures were  $9.4 \pm 0.3$  and  $11.9 \pm 0.3$  GPa. In this study, ZnTe-II was found to be a semiconductor with an optical gap of 2.5 eV at 9.5 GPa. In a combined electrical resistivity and volume change measurements<sup>11</sup> study, the authors observed a relatively large volume reduction at 9.0 and 12.0 GPa. They also suggested the possibility of another transition at lower pressure. In the first attempt to identify the high-pressure phases,<sup>5,6</sup> three x-ray-diffraction lines were observed in the pressure domain of ZnTe-III and the diatomic equivalent of  $\beta$ -tin was proposed for this phase. The indexation of ZnTe-II was not possible, even if the cinnabar structure is suggested.<sup>7</sup> In an unpublished x-ray-diffraction study cited in Ref. 12, ten diffraction peaks of ZnTe-III were indexed assuming a monoclinic structure. For ZnTe-II, indexation was still not possible,

but  $\beta$ -tin or rocksalt structures were excluded.

Other clues about the structure of the high-pressure phases of ZnTe have been found by comparison with the other zinc chalcogenides. Computations made by Chelikowski<sup>13</sup> show that the character of the high-pressure phase is strongly related to the atomic volume and ionicity. For ZnS, ZnSe, and ZnTe, these calculations show that the NaCl structure is more stable than the diatomic equivalent of the  $\beta$ -Sn one. NaCl is indeed the observed high-pressure phase of ZnS (Refs. 14 and 15) and ZnSe.<sup>14</sup> The dependence of the transition pressure on the atomic volume suggests that for ZnTe a change of coordination towards an octahedral environment can be expected below 13 GPa. This is in agreement with observations, but still leaves the two observed transitions as possible candidates for this change.

Determination of new structures at very high pressure has to overcome many difficulties. Diffraction experiments on single crystals are scarce, because phase transitions generally transform single crystals into polycrystalline samples. Therefore, experiments are mostly performed on powders for these determinations. In general, to attain pressures higher than 10–20 GPa, the geometry of high-pressure cells implies a limited angular access for diffraction studies. Other difficulties appear, such as pressure gradients in the cell, texture effects, or preferential orientation, which complicate the diffraction pattern making the indexation task difficult. On the other hand, because of the small size of the sample and of the diamond absorption, these experiments are very time consuming with classical x-ray sources and, in general, it is preferable to use synchrotron-radiation sources. Because of all the factors mentioned, one of the most convenient diffraction techniques when working at high pressures is energy dispersive diffraction with synchrotron-radiation sources. The symmetry of the crystal and the unit-cell parameters are the structural information which is most easily obtained. Unfortunately, the content of the unit cell is still difficult to obtain with only this technique alone, and other techniques are needed to get a better understanding of the structure of the high-pressure phases. High-pressure x-ray absorption provides a different type of information: the local structure. In crystalline materials, this allows us to get information directly from the unit cell, complementing the diffraction information currently available in high-pressure phases.

In this paper we report a combined *in situ* x-ray-absorption spectroscopy (XAS) and x-ray-diffraction study of the evolution of ZnTe at room temperature up to pressures of 30 GPa. XAS has proved to be especially well suited to probe the evolution of the local environment of atoms when subjected to high pressures. A list of more than 20 published papers concerning this subject recently appeared.<sup>16,17</sup> The number of neighbors in a shell, interatomic distances, and the pseudo-Debye-Waller factor are among the information present in a XAS spectrum.

In the present paper, the various experimental procedures are presented in Sec. II. The specific problems concerning XAS at high pressure are discussed in Sec. III. The results are presented and discussed to draw con-

clusions about the phase diagram of ZnTe in Sec. IV, finally, the general conclusions are drawn in Sec. V.

## II. EXPERIMENTAL PROCEDURE

### A. High-pressure apparatus

Membrane<sup>18</sup> or Block-Piermarini<sup>19</sup>-type diamond-anvil cells were used as high-pressure generators. The diamonds were of the Drukker standard type, with culets ranging from 0.5 to 1 mm in diameter. Fine grained powdered samples were loaded in 200–500- $\mu$ m-diameter holes drilled in stainless-steel gaskets.

In x-ray-absorption experiments, the size of the focused x-ray beam on the sample is about 0.5 mm, so that the use of gasket holes less than this diameter produces a supplementary collimation of the x-ray beam. In the experiments there is obviously a compromise between the maximum pressure attainable and the maximum number of photons on the sample.

Silicone oil was used as a pressure-transmitting medium. Alternatively, it would be possible to use a 4:1 methanol-ethanol mixture, but it solidifies in the 10-GPa region, where the transition between ZnTe-I and ZnTe-II takes place. The solidification of the pressure transmitting medium brings in inhomogeneous stresses which, as far as possible, must be avoided when it takes place around the transition pressure of the sample. Moreover, silicone oil is easier to manipulate when working with powder samples and this is very advantageous as time is an important variable in synchrotron-radiation facilities. The pressure was measured using the linear ruby fluorescence scale.<sup>20</sup>

### B. X-ray-absorption spectroscopy

Four experiments were performed, labeled *A1*, *A2*, *B1*, and *B2* in the following. In *A1* and *A2*, measurements were performed up to 15 GPa. In *A1*, the measurements were also performed on the downstroke, and in *A2* the sample was quenched from the highest attained pressure. *B1* and *B2* measurements were done up to 30 and 35 GPa, respectively, both during the upstroke and the downstroke. Unfortunately, in experiment *B2* only information about the edge position evolution with pressure could be extracted, due to the presence of many glitches of various origins in the spectra.

Experiments were performed at the dispersive x-ray-absorption station of Laboratoire pour l'Utilisation du Rayonnement Electromagnétique (LURE, Orsay, France) with the storage ring DCI operating at 1.85 GeV and 300–250 mA. Details of the experimental setup have been described elsewhere.<sup>21,22</sup> It consists essentially of a bent silicon crystal 22 cm long, which selects an energy band pass from the synchrotron white beam coming from a bending magnet. The x rays diffracted by the crystal establish a space-energy correlation and focuses the beam onto the sample with an intensity gain of 50 with respect to classical extended x-ray absorption fine structure (EXAFS) techniques. Detection is performed by a high-flux position-sensitive detector placed after the sample. The

incident and the transmitted x-ray intensities in the selected domain of energies are alternatively measured. Before detection, it is necessary to reject the harmonics of the selected energy domain. This is performed by a fused-silica mirror<sup>23</sup> placed between the sample and the detector. Harmonic rejection turns out to be essential in high-pressure experiments, because the beam passes through about 6 mm of diamond which will transmit the harmonics better than the selected energies and therefore deform the transmission spectrum. The optics of the station deserve some more comments because of special features which make the experimental setup very well suited for high-pressure experiments. In fact, thanks to the peculiar profile of the bent silicon crystal, aberration-free optics is attained.<sup>23</sup> This enables us to obtain the best performance in focusing in the plane of the orbit of the storage ring. In this way the energy distribution in the 500- $\mu\text{m}$  focalization spot is uniform enough to allow a collimation in the refereed plane down to the size of the gasket hole (which can be less than 200  $\mu\text{m}$ ). This is done almost without affecting the good energy distribution in the spot. In the vertical plane the beam is directly collimated without focalization. Because diamonds are single crystals, they diffract photons at given energies, bringing in glitches in the XAS spectra, which have to be rejected by orientation of the diamond-anvil cell with respect to the beam. A great advantage of the energy dispersive setup when working at high pressures is the real-time visualization of the spectrum, which allows easy rejection of diamond glitches.

Mechanical stability, focusing optics, harmonic rejection, and real-time visualization of the XAS spectrum are the main qualities that make the energy-dispersive mode especially well suited to be used in combination with a diamond anvil cell (DAC).<sup>24</sup> These qualities enable us to obtain high-quality XAS spectra under pressure.

The experiments were performed at the Zn *K* edge (9659 eV), using as dispersive optics a Si(111) crystal, which gives a band pass of about 700 eV. Orientation of the cell with respect to the beam was permitted to get rid of glitches coming from the diffraction of the diamonds away from a band pass of interest 400–600-eV wide.

### C. Energy-dispersive x-ray diffraction

X-ray-diffraction experiments were performed at the energy-dispersive x-ray setup at LURE. The white beam from the wiggler line of DCI was collimated down to 50  $\mu\text{m} \times 50 \mu\text{m}$  before the sample. After the DAC, a tungsten carbide slit 50 mm long was used to define the diffraction angle. A Ge multichannel detector explored the reciprocal space by analyzing the energy of the diffracted beam.

A single upstroke experiment was performed up to 23.5 GPa, allowing the determination of the equation of state (EOS) of ZnTe-I, the cell parameters of ZnTe-II, and the transition pressures.

## III. HIGH PRESSURE AND XAS

### A. X-ray-absorption near-edge structure (XANES)

It has been shown<sup>17,25</sup> that very important qualitative information can be obtained due to the XANES (about 50 eV above the edge) sensitivity to the local coordination, interatomic distances, and electronic configuration. Recent multiple-scattering calculations<sup>26</sup> have proved that to reproduce the Zn *K*-edge XANES of ZnS, it is necessary to consider neighbor shells around the absorber atom up to the fifth shell. This medium-range information complements the short-range information contained in the EXAFS part of the spectrum.

Independent of the experimental resolution, due to the core-hole lifetime, most of the detailed resonance peak structures appearing in multiple-scattering calculations are lost in the experimental spectrum. On the other hand, there is, up to now, no analytic form for the XANES multiple-scattering resonances and it is thus impossible to obtain a multiple-scattering resonance peak picture from the experimental spectrum. To get a quantitative image of the evolution of XANES with pressure, we have followed the position of the maxima of the observed XANES features with respect to the zero of energy for the photoelectron,  $E_0$  defined as in the EXAFS analysis, where it is associated with a particular feature at the edge. This has been taken, following usual conventions, as the first inflection point in the absorption edge.

### B. EXAFS

For a polycrystalline material, the EXAFS oscillations are reproduced by

$$\chi(k) = \sum_j \frac{N_j}{kR_j^2} |f_j(k, \pi)| \sin[2kR_j + \delta_j(k)] \times e^{-\sigma^2 k^2} e^{-2R_j/\lambda_j(k)}, \quad (1)$$

where  $N_j$  is the number of atoms in the  $j$ th neighboring shell at distance  $R_j$ ,  $|f_j(k, \pi)|$  is the backscattering amplitude,  $\lambda_j(k)$  the electron mean free path,  $\sigma_j^2$  (pseudo-Debye-Waller factor) the mean-square displacement from the equilibrium distances between the absorbing atom and atoms from the  $j$ th shell, and  $\delta_j(k)$  the total phase shift due to both the backscattering and the absorbing atom. The photoelectron wave vector  $k$  is given by

$$k = \hbar^{-1} [2m(E - E_0)]^{1/2}, \quad (2)$$

where  $E$  is the incident photoelectron energy,  $E_0$  the absorption edge energy, and  $m$  the electron rest mass. In Eq. (1), the structural parameters  $N_j$ ,  $R_j$ , and  $\sigma_j^2$  are pressure dependent, whereas the electronic functions  $|f_j(k, \pi)|$ ,  $\delta_j(k)$ , and  $\lambda_j(k)$  can be considered as pressure independent. Details of the data reduction of EXAFS data at high pressure have been presented elsewhere.<sup>17,25</sup>

In EXAFS analysis, the pseudo-Debye-Waller factor  $\sigma^2$  [by extension,  $\sigma^2$  and not  $\exp(-\sigma^2 k^2)$  will be called the pseudo-Debye-Waller factor] plays a major role in the data interpretation. In this term are included the static

and dynamic deviations from the equilibrium neighbor distances of the fitted structure. This information is, therefore, very valuable if one is able to separate both contributions. The easiest way to do this is to make experiments at various temperatures. Nevertheless, if the pressure dependence on the dynamic part of  $\sigma^2$  is known, it will also be possible to separate these terms by applying pressure on the sample. Experimentally, this can be done by combining temperature and pressure experiments, but such experiments have still not been performed. The full calculation of the evolution of the thermal part of the  $\sigma^2$  factor will imply the evaluation of lattice-dynamics models at any pressure.<sup>27</sup>

#### IV. RESULTS AND DISCUSSION

The four XAS experiments have been analyzed with the methods described above. In all experiments the EXAFS pair-pseudo-distribution functions (PPDF) show a doublet between approximately 1.5 and 3 Å. This signal is identified as coming from the first coordination shell surrounding Zn atoms. A signal from the second coordination shell (at 4.31 Å at ambient) is not seen under pressure. As the shift effects on the peak position in the PPDF due to the phase-shift function are generally less than 0.5 Å, any participation of second-neighbor shells in the 1.5–3 Å doublet is excluded. The origin of the doublet form of the first coordination shell contribution to the PPDF is the peculiar form of the EXAFS phase-shift and backscattering amplitude functions for Zn (absorber)-Te(scatterer) pairs. *Ab initio* calculations of these functions<sup>28</sup> have shown that when the involved atoms have high atomic numbers, resonances in the electron-atom scattering processes bring in peaks and valleys in the EXAFS atomic functions. The consequence is the apparition of doublets in the PPDF. All EXAFS fits will be referred to the information contained in this doublet, and therefore to the first coordination shell around Zn atoms.

X-ray-diffraction (Fig. 1), XANES (Figs. 2 and 3), and EXAFS (Fig. 4) analysis allow us to distinguish three different domains of behavior corresponding to the different observed phases that will be discussed separately.

##### A. ZnTe-I

Up to  $9.5 \pm 0.5$  GPa all experiments show the isotropic compression of the zinc-blende phase (ZnTe-I). The EXAFS oscillations and x-ray-diffraction peaks shift progressively to higher energies as expected from the decrease of the interatomic distances.

At ambient conditions, XANES at the Zn *K* edge shows a white line (WL), followed by three structures, labeled  $P_j$ ,  $j=1, 2$ , and 3 in the following (Fig. 2). The evolution of their position under pressure was followed with respect to the edge, except for  $P_2$  which is not well separated from  $P_3$ . XANES structures also shift to higher energies as can be seen from the variation of the observed maxima position of the white line and  $P_1$  in Fig. 3. This XANES shift has also been observed in multiple-

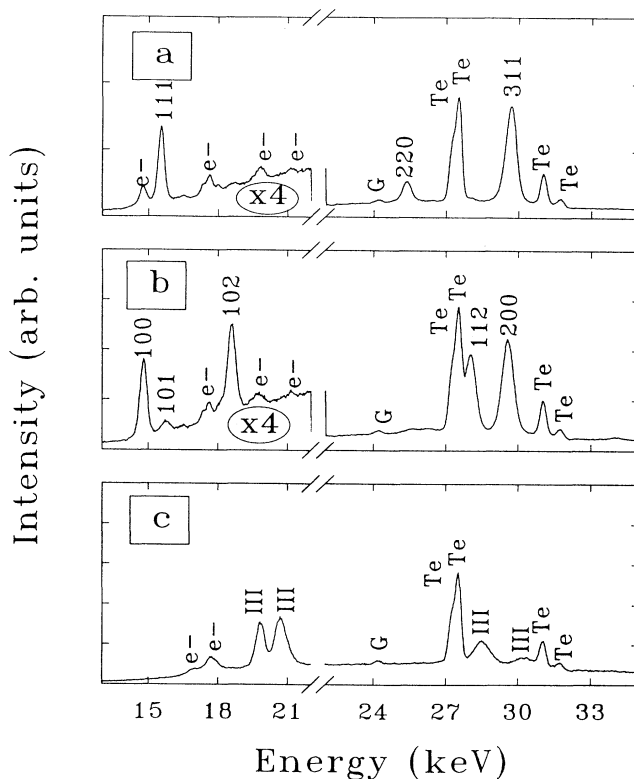


FIG. 1. Diffraction patterns in the three crystallographic phases. (a)  $P=8.4$  GPa, (b)  $P=11.7$  GPa, and (c)  $P=23.5$  GPa. The “Te” symbol states for fluorescence peaks from Te atoms, and “G” for a peak originated by the stainless-steel gasket. In (a) and (b), the intensities are multiplied by a factor of 4 at energies below 22 keV.

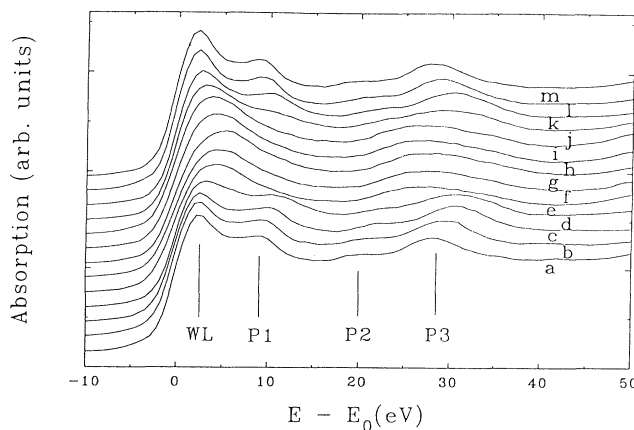


FIG. 2. XANES spectra in experiment B1. WL,  $P_1$ , and  $P_3$  are labels for the structures referred to in the text. Labels correspond to pressure as follows. Upstroke: (a) 0.4 GPa, (b) 3.4 GPa, (c) 8.9 GPa, (d) 11.5 GPa, (e) 14.9 GPa, (f) 21.1 GPa, (g) 29.2 GPa. Downstroke: (h) 20.0 GPa, (i) 15.3 GPa, (j) 11.5 GPa, (k) 8.9 GPa, (l) 3.1 GPa, (m) 0.4 GPa.

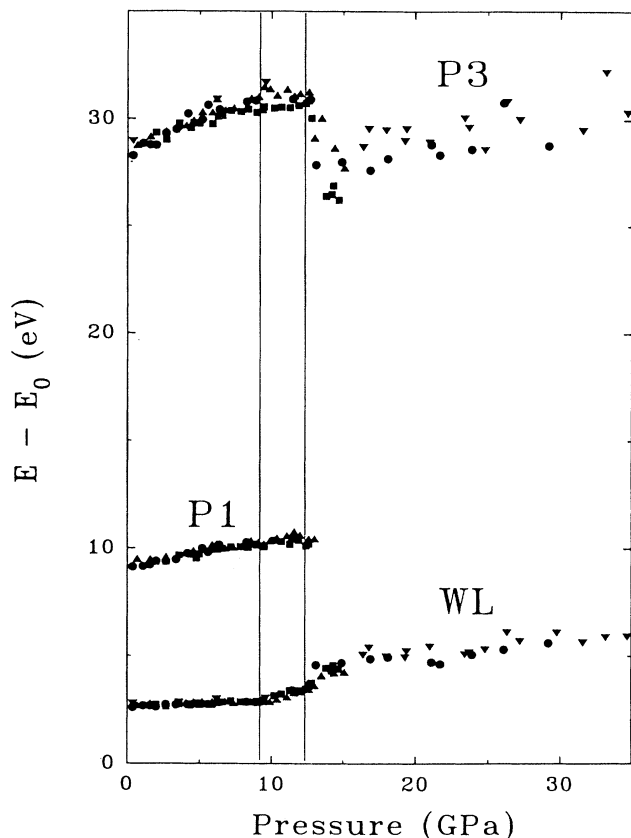


FIG. 3. Evolution of the position of the maximum of WL, P1, and P3 referred to the edge position. Solid figures: upstroke. Open figures: downstroke.

scattering calculations of ZnS (Ref. 26) at the Zn *K* edge, when decreasing distances between atoms. This is also the common observed behavior in other isotropically compressible materials such as ZnSe,<sup>29</sup> GaAs,<sup>30</sup> GaP,<sup>31</sup> and GaN.<sup>32</sup>

The contribution of the first coordination shell to the EXAFS PPDF shifts gradually its position to smaller dis-

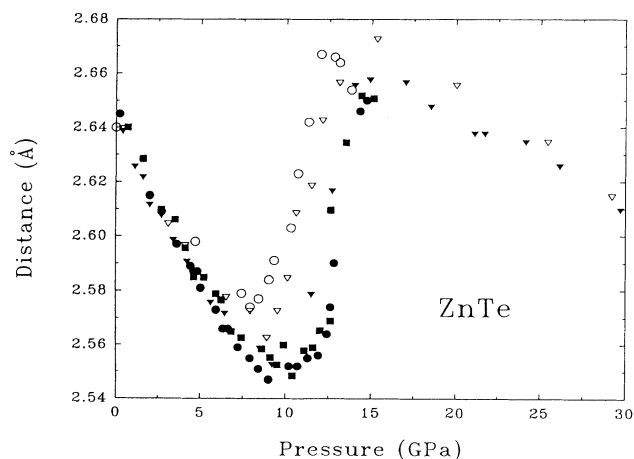


FIG. 4. First-neighbor distance obtained by EXAFS analysis as a function of pressure. Experiments are the following: A1 (circles), A2 (squares), and B1 (triangles). Solid figures denote upstroke and open figures denote downstroke.

tances in the pressure domain in discussion, and the intensity grows as expected from the decrease of the dynamical disorder. The accuracy in the observed  $\sigma^2$  variations is quite limited mainly due to the spectra normalization procedure. It is affected by the presence of diffraction glitches, which limits the extent of the usable energy domain above and below the edge. The values deduced from the three experiments are shown in Fig. 5.

It is possible to combine the Einstein approximation with Raman-scattering data under pressure to evaluate in a first-order approximation the evolution of the harmonic dynamic part of  $\sigma^2$ .<sup>33</sup>  $\sigma^2$  can be related to the LO mode frequency by

$$\sigma^2 = \frac{\hbar}{2\mu\omega_{\text{LO}}} \coth \left( \frac{\hbar\omega_{\text{LO}}}{2k_B T} \right), \quad (3)$$

where  $\omega_{\text{LO}}$  is the longitudinal-optical phonon frequency,  $\mu$  the reduced mass, and  $k_B$  the Boltzmann constant. If the Grüneisen parameter for the LO mode is known, the expected pressure dependence of the harmonic dynamic part of  $\sigma^2$  can be related to the first-neighbor distance variation by

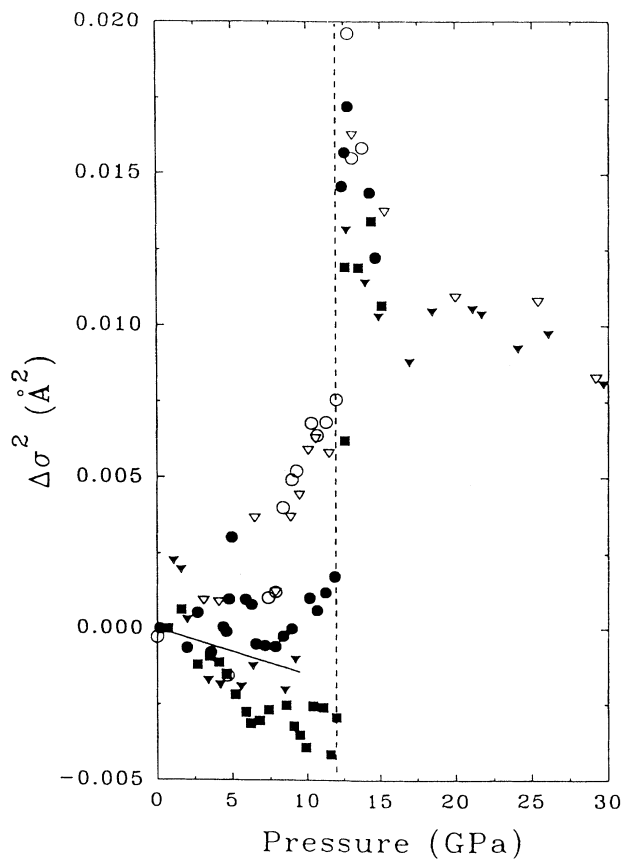


FIG. 5. Evolution of the pseudo-Debye-Waller factor with pressure. The dashed line at 12 GPa separates values obtained from fit with fourfold coordination from those with sixfold coordination. The line represents the variation of  $\Delta\sigma^2$  calculated using Eq. (4). Solid figures: upstroke. Open figures: downstroke.

$$\frac{\Delta\sigma^2}{\sigma^2} = 6\gamma_{LO} \frac{\Delta R}{R}, \quad (4)$$

where  $\gamma_{LO} = d \ln \omega_{LO} / d \ln P$  is the Grüneisen parameter. In ZnTe,  $\omega_{LO} = 206 \text{ cm}^{-1}$  and  $d\omega_{LO}/dP = 5.2 \text{ cm}^{-1} \text{ GPa}^{-1}$  from Raman experiments.<sup>34</sup> So the expected dependence of  $\Delta\sigma^2$  with pressure for an isotropic compression in an Einstein model is  $1.5 \times 10^{-4} \text{ \AA}^2 \text{ GPa}^{-1}$ . This dependence has also been plotted in Fig. 5 for comparison.

Figure 6 shows the evolution of the distances obtained by EXAFS analysis of the three experiments in the low-pressure phase. Points have been fitted with a first-order Murnaghan equation of state<sup>35</sup>

$$d = d_0 \left[ 1 + \frac{B'_0}{B_0} P \right]^{-1/3B'_0}. \quad (5)$$

Here,  $B_0$  is the bulk modulus at ambient,  $B'_0$  is its pressure derivative, and  $d_0$  is the interatomic distance at ambient. The best fit gives  $B_0 = 56 \pm 5 \text{ GPa}$  maintaining constant  $B'_0 = 5$  from ultrasonic experiments.<sup>36</sup>

In Fig. 6, the corresponding evolution of distances obtained from the unit-cell parameter in our x-ray-diffraction experiment is also shown. The best fit for this experiment was  $B_0 = 50.5 \text{ GPa}$  taking  $B'_0 = 5$ .

In Table I, the present results are compared with available published data. Our diffraction result for  $B_0$  is in very good agreement with the other values:  $B_0 = 50.8 \text{ GPa}$  from ultrasonics<sup>36</sup> measurements or  $B_0 = 50.9 \text{ GPa}$  from piezoelectric ones.<sup>37</sup> On the other hand, the EXAFS value for  $B_0$  is slightly higher. It is important to note that at 9 GPa, the difference between EXAFS and x-ray-diffraction values implies only a relative error of 0.4% for the interatomic distances, i.e., a difference of 0.01 Å. For pressures below 3 GPa, EXAFS results are

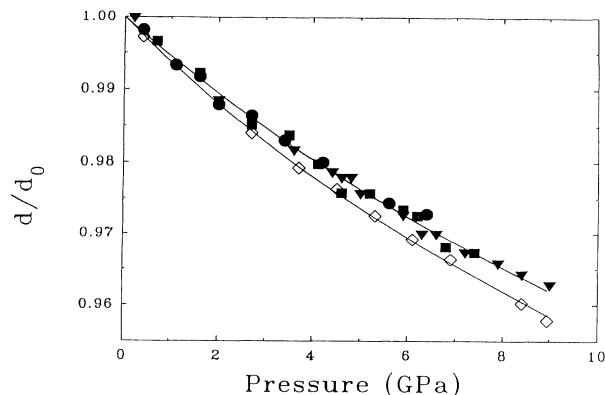


FIG. 6. Zn-Te distance normalized to ambient conditions in ZnTe-I as a function of pressure. Open figures: diffraction. Solid figures: EXAFS. Continuous line: first-order Murnaghan equation of state fitted to the experiments.

in very good agreement with diffraction ones (they give  $B_0 = 52 \pm 5 \text{ GPa}$  taking  $B' = 5$ ). A tentative explanation of the observed differences can be the nontransferability of the EXAFS phase-shift function due to the electronic changes observed between 3 and 5 GPa,<sup>5-7</sup> or to the decrease of distances. Other explanations are possible such as pressure gradient effects. In fact, XAS measurements are done over the whole sample volume, whereas diffraction ones only explore the central part of the experimental volume where it has been proved that the gradient effects are less important.<sup>38</sup> As the pressure decreases from the central part of the gasket hole, XAS measurements would give larger values of interatomic distances, as was observed. The importance of this effect

TABLE I. Experimental and theoretical results concerning some of the most important parameters of ZnTe high-pressure structural evolution.

Study	$B_0$ (GPa)	$B'_0$	$P_{\text{TI-II}}$ (GPa)	Structure ZnTe-II	$P_{\text{TI-III}}$ (GPa)	Structure ZnTe-III
Diffraction and electric resistivity <sup>a</sup>			8.5	hexagonal	13.0	$\beta$ -tin (metallic)
Ultrasound <sup>b</sup>	$50.8 \pm 0.7$	5.08				
Diffraction and optical absorption <sup>c</sup>	48.0	4.7	$9.4 \pm 0.3$		$11.9 \pm 0.3$	monoclinic
Electrostatic measurements <sup>d</sup>	50.9					
Calculations	$59^f, 52.1^g$	$4.61 \sim 4.98^h$	$18.8^j$			
X-ray diffraction <sup>e</sup>	50.5	5 <sup>i</sup>	$9.5 \pm 0.5$	hexagonal	$12.0 \pm 0.5$	
X-ray absorption <sup>e</sup>	50.5	5 <sup>i</sup>	$9.5 \pm 0.5$	local: fourfold coordination	$12.0 \pm 0.5$	local: distorted octahedron

<sup>a</sup>Reference 11.

<sup>b</sup>Reference 36.

<sup>c</sup>References 10 and 12.

<sup>d</sup>D. Berlincourt, H. Jaffe, and L. R. Shiozawa, Phys. Rev. **129**, 1009 (1963).

<sup>e</sup>This work.

<sup>f</sup>M. L. Cohen, Phys. Rev. B **32**, 7988 (1985)

<sup>g</sup>S. H. Wei and A. Zunger, Phys. Rev. B **37**, 8958 (1988).

<sup>h</sup>T. Soma, Y. Takahashi, and H. Matsuo Kagaya, Solid State Commun. **53**, 801 (1985).

<sup>i</sup>Fixed.

<sup>j</sup>N. E. Christensen and O. B. Christensen, Phys. Rev. B **33**, 4769 (1986).

would increase with pressure, which is the case in this study.

### B. ZnTe-II

In the x-ray-diffraction measurements, the destabilization of ZnTe-I is clearly seen by the presence of new peaks from 9.7 GPa which are not seen at 9.3 GPa. The transformation seems to be completed at 11.7 GPa where a total of 7 characteristic peaks are identified for ZnTe-II. Some of these peaks are approximately at the same positions as in ZnTe-I or ZnTe-III (Fig. 7), and are broader than the ZnTe-I ones. This effect has also been noted in angular dispersive x-ray diffraction.<sup>39</sup> It is not possible from the present experiments to deduce the origin of this broadening. At 12.1 GPa the presence of new peaks indicates the end of the stability domain of ZnTe-II.

In the XAS experiments, the end of the ZnTe-I stability domain is observed by the change of the pressure dependence of the first-neighbor distance and XANES in experiments A1 and A2. From the changes in both parts of the XAS spectra, the destabilization of ZnTe-I begins at  $9.5 \pm 0.5$  GPa, as shown in Figs. 3 and 4. The new regime remains until  $12 \pm 0.5$  GPa.

XANES spectra in the ZnTe-II zone retain all the features pointed out in ZnTe-I, but (i) a change of slope

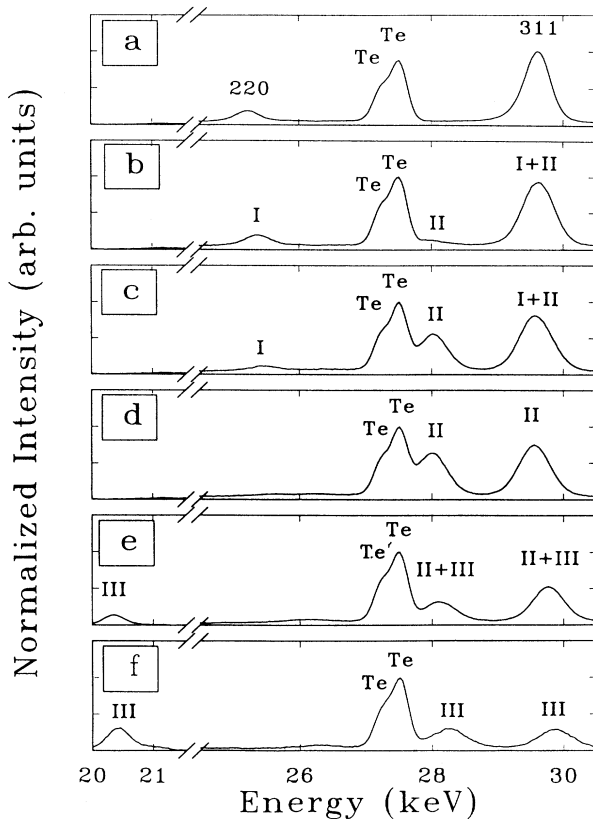


FIG. 7. Normalized x-ray-diffraction partial patterns taken in the phase transition regions. (a)  $P=8.4$  GPa, (b)  $P=9.4$  GPa, (c)  $P=11.2$  GPa, (d)  $P=11.7$  GPa, (e)  $P=13.2$  GPa, (f)  $P=15.4$  GPa.

does appear in the evolution of the position of the white line (Fig. 3), and (ii) the white line and  $P_1$  widen considerably (Fig. 2). Due to the proximity of ZnTe-III, the first question to answer is if the observed changes can be explained by a phase mixture between ZnTe-I and ZnTe-III. In case of the presence of two different phases, it is possible to reproduce the XANES part by a weighted average of two spectra from the pure phases taken near the transition pressure, as has been done for  $\text{GeO}_2$ ,<sup>24</sup> and for GaAs.<sup>30</sup> All trials to reproduce the XANES spectrum in this pressure range using such a procedure failed to produce the observed broadening of  $P_1$  (Fig. 8).

The quality of the EXAFS fits decreases only slightly in this zone, but remains reasonably good taking a fourfold-coordinated polyhedron (Fig. 8). Three types of local structures were tested. We tried 4 or 6 Te atoms at the same distance or 4 Te atoms at two different distances. Only did the case of fourfold coordination show a consistent evolution both in distance and in the pseudo-Debye-Waller and give relatively good fits (Fig. 9).

It has been observed by Raman spectroscopy<sup>9</sup> that there is a very narrow pressure domain (between 9.8 and 10.7 GPa) where ZnTe-II is the only phase present. As the determined distances in phases I and II are very close and no significant change in  $\Delta\sigma^2$  is observed, we conclude that ZnTe-II is fourfold coordinated, with four tellurium atoms around each Zn one. XANES similarities between ZnTe-I and ZnTe-II strengthen the fourfold-coordination assignment for ZnTe-II.

The x-ray-diffraction spectra of ZnTe-II may be indexed as a hexagonal structure with a  $c/a$  ratio equal to 2.272 at 11.7 GPa (see Table II). These values are to be compared with the values obtained in the similar compounds of cinnabar structure HgS: 2.288,<sup>40</sup> HgTe: between 2.28 at 2.8 GPa and 2.31 at 7.4 GPa,<sup>41</sup> HgO: 2.427,<sup>42</sup> or CdTe: 2.385 at 3.5 GPa.<sup>43</sup> It is justified to make the hypothesis that ZnTe-II has the cinnabar structure as already suggested in Ref. 7. The EXAFS data

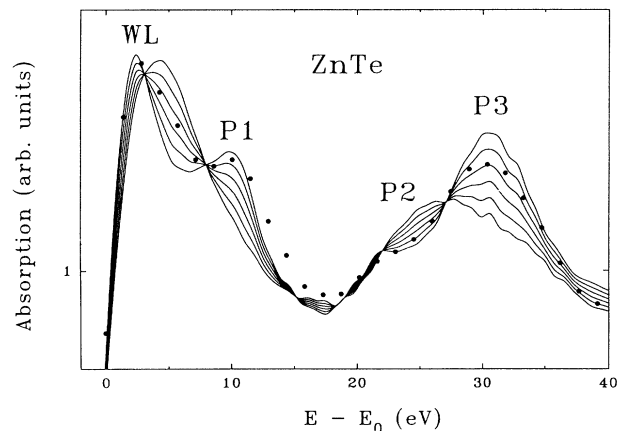


FIG. 8. Lines: XANES spectra obtained by weight averaging (0%, 20%, 40%, 60%, 80%, and 100%) the spectra at 8.9 GPa (ZnTe-I) and 14.9 GPa (ZnTe-II). Circles: spectrum at 11.5 GPa (ZnTe-II). The observed broadening of  $P_1$  is not reproduced in the phase mixture simulation. The labels are the same as in Fig. 2.

TABLE II. Comparison of experimental and calculated  $d_{hkl}$  for ZnTe-II at 11.7 GPa indexed in the cinnabar structure with  $a=4.066$  Å and  $c=9.25$  Å.

$hkl$	Calculated $d$ (Å)	Observed $d$ (Å)
100	3.521	3.517
101	3.291	3.304
102	2.802	2.799
112	1.861	1.859
200	1.761	1.761
203	1.529	1.529
212	1.279	1.278

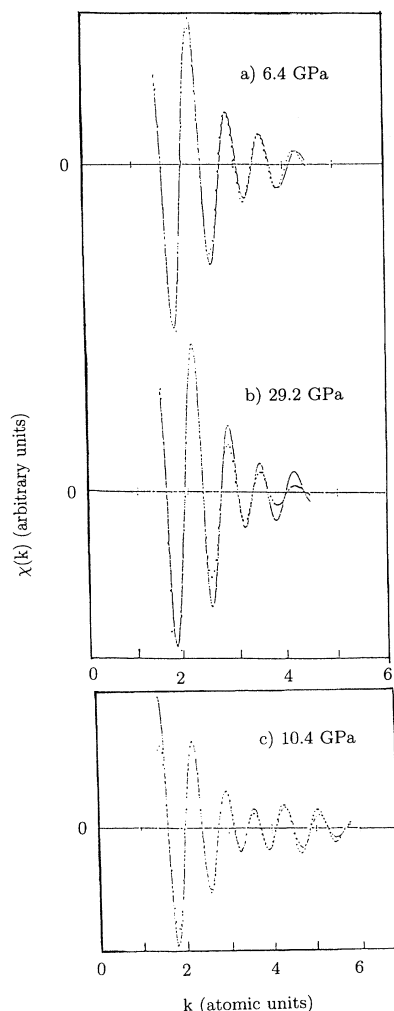


FIG. 9. First-neighbor filtered EXAFS oscillations at various pressures. The continuous line is the experimental spectrum and the dotted line is the fit using Eq. (1). (a) and (b) are from experiment *B1*; (c) is from *A2*. Fits were obtained with the following local structures: (a) 6.4 GPa, four Te neighbors at 2.57 Å; (b) 29.2 GPa, 6 Te neighbors at 2.61 Å; (c) 10.4 GPa, four Te neighbors at 2.55 Å.

show that the Zn atoms have four first neighbors. Therefore, the crystallographic parameters  $u$  and  $v$  of the cinnabar<sup>42</sup> structure are nearly equal ( $u=v=0.474$ ). Hence, the third-neighbor distance may be evaluated and is of the order of 3.7 Å. This distance is well outside of the peak corresponding to the first neighbors in the pair-pseudo-distribution function, and this explains why the EXAFS data could be fitted with four neighbors. Moreover, the first-neighbor distance in ZnTe-II is very near to that in the blende phase. This is in agreement with the blende→cinnabar transition in HgTe where the first-neighbor distance is almost the same in both phases.<sup>41</sup>

The volume compression at the transition is of the order of 13% at the blende→cinnabar transition and again 13% at the II→III transition. This is entirely consistent with the volume compression observed at the blende→cinnabar transition for HgTe (10.6%) (Ref. 41) and CdTe (13.3%).<sup>43</sup> Moreover, in the zinc chalcogenides where the cinnabar intermediate phase does not exist, the volume variation at the blende→NaCl transition is of the order of 25%. The cinnabar phase appears as an intermediate phase between the low-pressure fourfold-coordinated phase (blende) and the high-pressure sixfold-coordinated phase. Our diffraction and XAS transition pressure values are in perfect agreement with those obtained in Ref. 10.

### C. ZnTe-III

A ZnTe-II and ZnTe-III phase mixture was observed between 12.4 and 13.2 GPa by x-ray diffraction (Fig. 7). From 14.3 up to 23.5 GPa, the observed diffraction pattern was that of a single phase with five characteristic peaks. Between 11.9 and 14.9 GPa a rise in the first-neighbor distance of about 0.1 Å (Fig. 4) is accompanied by a dramatic change in XANES (Figs. 2 and 3). This is evidence of a transition to a new phase with an increase of the coordination number. This is also seen in the evolution of  $\Delta\sigma^2$  which shows a large increase, only interpretable as the consequence of the apparition of static disorder coming from a phase mixture (Fig. 5).

In this transition zone, we tried to fit the EXAFS signal by freezing the number of Te first neighbors to 4 or 6. This had practically no effect on the value of the obtained distances, but at higher pressure the fits with six neighbors were progressively better at the expense of the initially better fits with four neighbors. For pressures above 15 GPa, an octahedral polyhedron of coordination turns out to be clearly the best choice of local structure. From this value of pressure  $\Delta\sigma^2$  decreases. In a first step, this is interpreted as the disappearance of the static disorder, a consequence of the stabilization of ZnTe-III. In a second step, this evolution represents the decrease of the dynamic disorder from the compression of ZnTe-III that continues up to 30 GPa. In this domain, between 15 and 30 GPa, a shift of the edge position towards lower energies of about 0.5 eV is observed.

Three different local structures between 15 and 30 GPa were tested: (i) six Te atoms, (ii) four Te atoms and two Zn atoms, and (iii) four Te atoms and two Te atoms at different distances. We did not test other combinations

that could introduce too many degrees of freedom in our fits. Only option (i) showed a coherent evolution both in distances and in  $\Delta\sigma^2$ . But the quality of the fits is not very good and the obtained values of  $\Delta\sigma^2$  are very large for a single coordination shell. This last point can be seen from Eqs. (3) and (4) which, using the Raman data,<sup>34</sup> give a  $\Delta\sigma^2=0.0012 \text{ \AA}^2$  for the observed  $\Delta R$  at the transition. The observed value is  $\Delta\sigma^2\approx 0.01 \text{ \AA}^2$ . The discrepancy between our observation and the Einstein model is probably due to the anharmonicity or to a distribution of distances inside the shell. According to Ref. 6, ZnTe-III has a monoclinic structure. This is compatible with a distortion of a perfect octahedron, and would explain the low quality of the fits in this phase. Another fact strengthening this hypothesis is the comparison of ZnTe-III with the rocksalt-type high-temperature phase (ZnTe-IV). This phase has been found in a recent x-ray-diffraction study at temperatures above 200 °C by heating ZnTe-II.<sup>44</sup> At  $P=11.6 \text{ GPa}$  and  $T=400 \text{ }^\circ\text{C}$ , the unit-cell parameter of ZnTe-IV is  $5.502 \text{ \AA}$ . A fit with a Murnaghan EOS of the distance vs pressure in ZnTe-III gives  $B_0=145 \text{ GPa}$  with  $B'_0$  fixed to 5. If we suppose a rocksalt structure for ZnTe-III, the unit-cell parameter will be  $5.37 \text{ \AA}$  at 11 GPa. This value will be slightly larger at 400 °C. It is only 2.5% lower than the ZnTe-IV one. We conclude that the volumes of ZnTe-III and ZnTe-IV are very close, as well as their local structures. Moreover, if we extrapolate the Murnaghan EOS in ZnTe-I and ZnTe-III to the coordination change transition pressure (ignoring the ZnTe-II phase), the relative volume change would be  $\Delta V/V=0.26$  just after the transition. This value is very close to the reported ones for ZnS (Ref. 15) ( $\Delta V/V=0.27$ ) and ZnSe ( $\Delta V/V=0.28$ ).<sup>5</sup>

#### D. Reversibility

As was pointed out above, in two of the XAS experiments the downstroke has been studied. This allows us to follow the reverse transitions. As hysteresis is a common process in displacive transitions, it is necessary to study the forward and reverse transition<sup>30</sup> to determine the thermodynamic phase-transition pressures. In ZnS and ZnSe, the reverse transition between the rocksalt and the zinc-blende phase takes place without hysteresis.<sup>29</sup> In ZnTe the study is complicated by the presence of the intermediate ZnTe-II, a phase with a small domain of existence.

In all runs, the sample comes entirely back to the initial structure at ambient, showing no sign of amorphization. Even in the quenched sample the only significant difference with ZnTe before pressurization is a variation in the intensity of the white line (Fig. 10), which is probably due to the difference of thickness between the sample before and after the pressure cycle. In fact, the effect of the sample thickness is well known in classic EXAFS,<sup>45</sup> having its origin in the fact that even a "monochromatic" x-ray beam can contain wavelengths well away from the central peak. In dispersive EXAFS as in classical EXAFS the most important source of contamination of the beam is spurious harmonics which are not completely rejected. After attenuation by the strong absorption of the

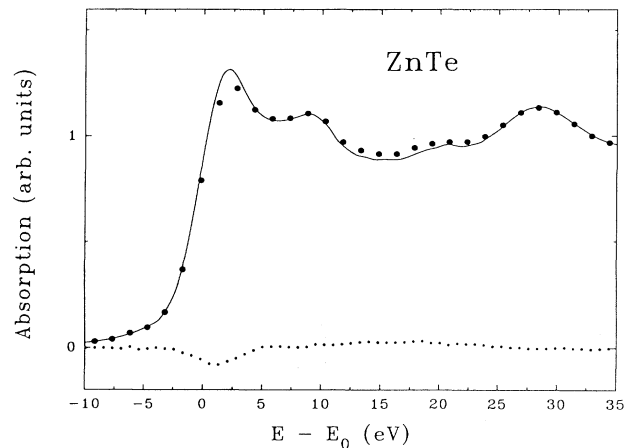


FIG. 10. Points: spectrum before pressurization. Continuous line: spectrum at  $P=0$  of the sample quenched from 15 GPa. Dotted line: difference between both spectra.

white line, the transmitted beam is dominated by the high-energy part, making the white line sensitive to thickness. Effects of the nonlinearity of the detector response to the photon flux may also be involved in this effect.

The destabilization of phase III when releasing the pressure is especially well seen in experiment B1. After reaching 15 GPa, we waited 12 h before starting to release pressure. EXAFS and XANES showed that, after this lapse of time, the sample was completely transformed into ZnTe-III. The first points of the downstroke evolve in this phase (Fig. 6). At  $12.2\pm 0.5 \text{ GPa}$ , distances start to decrease and the  $\sigma^2$  to increase. From this pressure the sample enters a phase mixture domain.

Due to phase mixture, it is difficult to establish if ZnTe-II is attained after ZnTe-III destabilization. In Fig. 3 it is possible to appreciate that on downstroke, when compared with the upstroke, the position of the white line is slightly shifted to a higher energy between 15 and 8 GPa. In Fig. 4 we observe that in this region the first-neighbor distance is at least  $0.02 \text{ \AA}$  longer than in the upstroke. Both observed effects in XANES and EXAFS evidence the presence of ZnTe-III in this pressure domain.

From 8 GPa both XANES and distances show the characters of the regime of fourfold coordination observed in ZnTe-I. This is also confirmed by the  $\sigma^2$  evolution (Fig. 5).

#### E. Edge evolution

The position of the absorption edge  $E_0$  is also a structural and electronic dependent feature of the XANES spectra. The energy  $E_0$  is indeed related to the energy of the first unoccupied electron states with the symmetry allowed by the dipolar selection rules ( $p$  symmetry for a  $K$  edge). This relation cannot be directly done because of multielectronic effects such as the presence of the core-hole potential which modifies the band

structure during the absorption process. Anyway, the position of the edge can be sensitive to the structural changes observed in high-pressure studies.

In two of the experiments the evolution of the position of the Zn *K* edge has been followed up to 30 GPa. As noted above, the position of the edge  $E_0$  has been taken at the first inflection point in the absorption edge. To determine the  $E_0$  evolution, we have to correct for possible shifts due to the effect of the x-ray beam fluctuations in the dispersive optics. This can be done following the  $E_0$  evolution with respect to the  $E_0$  position of a reference. We have taken as references the Zn *K* edge in a foil of metallic Zn or in a powdered sample of ZnTe at ambient. One of these references was measured after each measurement, enabling us to correct the effects of the synchrotron beam evolution. In case of important observed fluctuations, the experimental points were rejected. So as to evaluate the resolution in the determination of the relative position of  $E_0$ , in one of the experiments we took the two mentioned references after each absorption measurement. The difference between the position of the Zn *K* edge in ZnTe at ambient and in metallic Zn was of 1.55 eV. The accuracy of this determination is difficult to evaluate because of all possible systematic errors that can occur. When studying the evolution with pressure of the Zn *K* edge in ZnTe, the only clearly reproducible fact in all experiments was a shift to lower energies of the edge associated with the change of coordinance. This shift value is  $0.75 \pm 0.25$  eV. This means a large change in the band structure, as is expected from the metallization.

## V. CONCLUSION

ZnTe has been studied up to 30 GPa showing a succession of three crystallographic phases. As is shown in Table I, the present study confirms the values of the transition pressures presented in Ref. 12. In Ref. 7 the values are slightly different. Our x-ray-diffraction value for the

bulk modulus in ZnTe-I is in very good agreement with previous work. EXAFS analysis gives a value 10% larger. We have proposed some possible origins of this difference. Anyway, at 9 GPa this means a difference in first-neighbor distances of only 0.01 Å.

Interpretation of x-ray diffraction and XAS gives the same values for the transition pressures. At  $9.5 \pm 0.5$  GPa the zinc-blende phase becomes unstable giving place to a new phase. The combination of EXAFS and diffraction data led to the conclusion that this phase is similar to cinnabar, as in HgTe, but with the crystallographic parameters  $u$  and  $v$  nearly equal, i.e., there are four first neighbors, at nearly the same distance, the third pair of neighbors being much farther. At  $12.0 \pm 0.5$  GPa fourfold coordination is no longer stable and a transition occurs toward an octahedral configuration with 6 Te atoms surrounding each Zn atom. This octahedron is probably distorted. The structure seems to be stable up to 30 GPa and the reverse transition occurs without structural hysteresis. The way this reverse transition takes place is difficult to ascertain, but anyhow the sample does not completely come back to ZnTe-I at least until 8 GPa. The global process is structurally reversible and shows no amorphization.

## ACKNOWLEDGMENTS

One of us (A.S.M.) was supported by a grant from the Spanish Ministerio de Educacion y Ciencia. The samples were grown and supplied by R. Triboulet (Laboratoire de Physique des Solides de Bellevue). We are indebted to Dr. R. Nelmes and Dr. M. I. McMahon from the University of Edinburgh, Dr. K. Syassen from the Max Planck Institut of Stuttgart, and Dr. O. Shimomura from NIRIM, Tsukuba, for providing details on their x-ray-diffraction results on ZnTe before publication. Physique des Milieux Condensés is Unité Associée au Centre National de la Recherche Scientifique No. 782.

<sup>1</sup>M. T. Yin and M. L. Cohen, Phys. Rev. Lett. **45**, 1004 (1980).

<sup>2</sup>G. Kress and J. Hafner, Phys. Rev. B **47**, 558 (1993).

<sup>3</sup>S. Larachs, R. E. Sharader, and C. F. Stocker, Phys. Rev. **108**, 587 (1957).

<sup>4</sup>G. A. Samara and H. G. Drickamer, J. Phys. Chem. Solids **23**, 124 (1962).

<sup>5</sup>P. L. Smith and J. E. Martin, Phys. Lett. **19**, 541 (1965).

<sup>6</sup>A. Ohtani, M. Motobayashi, and A. Onodera, Phys. Lett. **75A**, 435 (1980).

<sup>7</sup>A. Onodera, A. Ohtani, T. Seike, M. Motobayashi, O. Shimomura, and H. Kawamura, in *Solid State Physics under Pressure*, edited by S. Minomura (Terra Scientific, Tokyo, 1985), p. 141.

<sup>8</sup>M. Linder, G. F. Schötz, P. Link, H. P. Wagner, W. Kuhn, and W. Gebhardt, J. Phys. Condens. Matter **4**, 6401 (1992).

<sup>9</sup>C. Abraham, Thesis, University of Stuttgart, 1992 (unpublished).

<sup>10</sup>K. Strössner, S. Ves, Chul Koo Kim, and M. Cardona, Solid State Commun. **61**, 275 (1987).

<sup>11</sup>S. Endo, A. Yoneda, M. Ichikawa, S. Tanaka, and S. I. Kawabe, J. Phys. Soc. Jpn. **51**, 138 (1982).

<sup>12</sup>K. Strössner, S. Ves, W. Hönlle, W. Gebhardt, and M. Cardona, in *Proceedings of the 18th International Conference on the Physics of Semiconductors, Stockholm, 1986*, edited by O. Engström (World Scientific, Singapore, 1987), p. 1717.

<sup>13</sup>J. R. Chelikowski, Phys. Rev. B **35**, 1174 (1987).

<sup>14</sup>P. L. Smith and J. E. Martin, Phys. Lett. **19**, 541 (1965).

<sup>15</sup>S. Ves, U. Schwarz, N. E. Christensen, K. Syassen, and M. Cardona, Phys. Rev. B **42**, 9113 (1990).

<sup>16</sup>J. Freund, R. Ingalls, and E. D. Crozier, Phys. Rev. B **43**, 9894 (1991).

<sup>17</sup>J. P. Itié, Phase Transitions **39**, 81 (1992).

<sup>18</sup>R. Le Toullec, J. P. Pinceaux, and P. Loubeyre, High Pressure Res. **1**, 77 (1988).

<sup>19</sup>G. J. Piermarini, S. Block, J. D. Barnett, and R. A. Forman, J. Appl. Phys. **46**, 2774 (1975).

<sup>20</sup>G. J. Piermarini and S. Block, Rev. Sci. Instrum. **46**, 973 (1975).

- <sup>21</sup>E. Dartyge, C. Depautex, J. M. Dubuisson, A. Fontaine, A. Jucha, and G. Tourillon, *Nucl. Instrum. Methods A* **246**, 452 (1986).
- <sup>22</sup>H. Tolentino, E. Dartyge, A. Fontaine, and G. Tourillon, *J. Appl. Crystallogr.* **21**, 15 (1988).
- <sup>23</sup>H. Tolentino, F. Baudelet, E. Dartyge, A. Fontaine, A. Lena, and G. Tourillon, *Nucl. Instrum. Methods A* **286**, 307 (1990).
- <sup>24</sup>J. P. Itié, A. Polian, G. Calas, J. Petiau, A. Fontaine, and H. Tolentino, *Phys. Rev. Lett.* **63**, 398 (1989).
- <sup>25</sup>J. P. Itié, A. San-Miguel, and A. Polian, *Jpn. J. Appl. Phys.* **32**, 711 (1993).
- <sup>26</sup>P. Sainctavit, J. P. Itié, A. Polian, and A. San-Miguel, *Jpn. J. Appl. Phys.* **32**, 44 (1993).
- <sup>27</sup>E. Sevillano, H. Meuth, and J. J. Rehr, *Phys. Rev. B* **20**, 4908 (1979).
- <sup>28</sup>B. K. Teo and P. A. Lee, *J. Am. Chem. Soc.* **101**, 2815 (1979).
- <sup>29</sup>J. P. Itié, A. San-Miguel, and A. Polian (unpublished).
- <sup>30</sup>J. M. Besson, J. P. Itié, A. Polian, G. Weill, J. L. Mansot, and J. Gonzalez, *Phys. Rev. B* **44**, 4212 (1991).
- <sup>31</sup>J. P. Itié, A. Polian, C. Jauberthie-Carillon, E. Dartyge, A. Fontaine, H. Tolentino, and T. Tourillon, *Phys. Rev. B* **40**, 9709 (1989).
- <sup>32</sup>P. Perlin, C. Jauberthie-Carillon, J. P. Itié, A. San-Miguel, I. Gzegory, and A. Polian, *Phys. Rev. B* **45**, 83 (1992).
- <sup>33</sup>J. M. Tranquada, R. Ingalls, and E. D. Crozier, in *EXAFS and Near Edge Structure III*, edited by K. O. Hodgson, B. Hedman, and J. E. Penner-Hahn (Springer-Verlag, Berlin, 1984), p. 374.
- <sup>34</sup>J. R. Ferraro, *Vibrational Spectroscopy at High External Pressures* (Academic, New York, 1984).
- <sup>35</sup>F. D. Murnaghan, *Proc. Natl. Acad. Sci. U.S.A.* **30**, 244 (1944).
- <sup>36</sup>B. H. Lee, *J. Appl. Phys.* **41**, 2988 (1970).
- <sup>37</sup>D. Belincourt, H. Jaffe, and L. R. Shiozawa, *Phys. Rev.* **129**, 1009 (1963).
- <sup>38</sup>A. Ruoff, *High Pressure Res.* **1**, 3 (1988).
- <sup>39</sup>R. Nelmes, private communication.
- <sup>40</sup>K. L. Aurivillius, *Acta Chem. Scand.* **4**, 1413 (1950).
- <sup>41</sup>A. San-Miguel, J. P. Itié, A. Polian, R. J. Nelmes, M. I. McMahon, and N. G. Wright (unpublished).
- <sup>42</sup>R. W. G. Wyckoff, *Crystal Structures* (Krieger, Malabar, 1982).
- <sup>43</sup>R. J. Nelmes, M. I. McMahon, N. G. Wright, and R. Allan (unpublished).
- <sup>44</sup>O. Shimomura, private communication.
- <sup>45</sup>S. M. Heald and E. A. Stern, *Phys. Rev. B* **16**, 5549 (1977).